Coaxial Nozzle for Control of Particle Morphology in Precipitation with a Compressed Fluid Antisolvent

SIMON MAWSON, SANJAY KANAKIA, KEITH P. JOHNSTON

Department of Chemical Engineering, University of Texas, Austin, Texas 78712-1062

Received 6 April 1996; accepted 5 August 1996

ABSTRACT: A coaxial nozzle was developed to achieve further control over the morphology of microparticles precipitated from solution by carbon dioxide as a compressed fluid antisolvent. The polymer solution was sprayed through the core of the nozzle and CO_2 through the annulus. For the coaxial nozzle versus a standard nozzle, polystyrene and poly(L-lactic acid) particles can be larger by a factor of 3–8 with less flocculation. A reduction in the Weber number reduces atomization and larger droplets are formed in the jet, delaying precipitation. However, because of the much higher Reynolds number for the high velocity CO_2, the mass transfer in the suspension outside of the jet is faster leading to less flocculation and agglomeration. For polyacrylonitrile, the delayed precipitation produces a transition from highly oriented microfibrils to microparticles.
 J Appl Polym Sci **64:** 2105–2118, 1997

Key words: microparticles; compressed fluid antisolvent; coaxial nozzle; carbon dioxide

INTRODUCTION

Uniform polymeric microspheres and microparticles from 0.1 to 10 μm are of interest in many applications,[1] including microencapsulated pharmaceuticals for controlled drug delivery.[2] Microparticles can be produced with micronizers, for example, by jet milling,[3] but it is difficult to control particle size distributions and morphology and to avoid losses of material. Recently, spray processes with compressed fluids, including supercritical fluids, have achieved considerable success in addressing these problems. These include rapid expansion from a supercritical solution (RESS),[4–11] gas antisolvent crystallization (GAS),[12] and precipitation with a compressed fluid antisolvent (PCA).[13–22] In the antisolvent process, the biological activity of proteins, peptides, and enzymes was maintained.[18]

CO_2 is of interest as a solvent because it is inexpensive, essentially nontoxic, nonflammable, and environmentally acceptable. In addition, the temperature and pressure critical conditions, T_c = 31°C and P_c = 73.8 bar, are easily accessible. However, because CO_2 has no dipole moment and a low polarizability, it dissolves very few polymers.[23] Consequently, the use of RESS for polymers in CO_2 has been limited,[10,24] although a soluble high molecular weight fluoroacrylate has been sprayed to form particles and fibers.[11]

For processing polymers, CO_2 can be more effective as an antisolvent (also called nonsolvent) than as a solvent. In PCA, the CO_2 antisolvent may be a gas, liquid, or supercritical fluid, which is miscible with the organic solvent. The polymeric solution is atomized into flowing CO_2 through a 50–100 μm capillary,[14,15] an orifice,[18] or a sonication nozzle.[16,25] Diffusion coefficients of CO_2 into polymers and solvent into CO_2 are much larger than for conventional liquid antisolvents.

Correspondence to: K. P. Johnston.
Contract grant sponsor: National Science Foundation; contract grant number: CTS-9218769.
Contract grant sponsor: Texas Advanced Technology Program; contract grant number: 3658-198.

Table I Summary of Polymeric Microparticles Produced by PCA

Polymer (Solvent)	Concentration (wt %)	T (°C)	P (bar)	Q (Solution) (mL/min)	Q (CO_2) (mL/min)	Primary Particle (μm)	Macrostructure
PS (toluene)	1.0	0.3–25	40–135	> 0.5	> 35	~ 0.1	Flocculated cobweb
		30–40	73–225	> 0.5	> 35	~ 0.1–3.0	10–20 μm agglom.
	2.5	22	80.3	> 0.5	> 35	~ 0.1–3.0	Sl. flocc./agglom., cobweb
L-PLA (CH_2Cl_2)	0.6	31	75.8	1.0	405	0.3–1.0	Sl. flocc./agglom.
		31	82.7	1.0	367	0.6–1.3	Sl. flocc./agglom.
		31	96.5	1.0	342	1.1–1.7	Sl. flocc./agglom.
	1.0	31	82.7	1.0	367	0.6–1.3	Sl. flocc./agglom.
PC/SAN[a] (THF)	0.5	23	107	1.0	35	0.1–1.0	Sl. flocc./agglom.
	3.0	23	107	1.0	35	> 10.0	Sl. flocc./agglom., fibrous
Insulin (DMSO/DMF)	15[b]	25	86.2	0.3	17.2	2.4–2.7	Sl. flocc./agglom.
		35	86.2	0.3	21.6	1.9–3.8	Sl. flocc./agglom.

[a] Polycarbonate/poly(styrene-*co*-acrylonitrile) blends.
[b] mg/mL.

Because of the small process length scale created by jet atomization and the rapid two-way mass transfer, the phase separation is extremely fast, down to 10^{-5} s. This rate is at least 2 orders of magnitude faster than for the case of conventional liquid antisolvents, and approaches that of RESS.[22] Consequently, PCA may be used to produce high surface area materials, which can be quenched in a glassy or crystalline state before the surface area relaxes.[14]

Table I provides a summary of the various polymer/solvent systems that were processed into microparticles by PCA. By changing the solution concentration, CO_2 temperature, and the relative CO_2 to solution flow rate, 0.1–4.0 μm microspheres and microparticles of amorphous polystyrene (PS),[13–15] semicrystalline poly(L-lactic acid) (L-PLA),[16,21] biologically active insulin,[18] and metastable blends of polycarbonate/poly(styrene-*co*-acrylonitrile)[22] were formed. Previously, while observing sprays from a capillary atomization nozzle, we noticed refractive index gradients due to stratification of suspended solvent droplets.[20] The atomized droplets were not circulated very efficiently throughout the volume of the precipitation vessel. The resulting microparticles of amorphous polymers including PS, and to a much lesser extent semicrystalline polymers such as L-PLA were flocculated and somewhat agglomerated.

The objective of this study is to utilize a coaxial nozzle in the PCA process to achieve further control over the product morphology and to better understand the hydrodynamic and mass transfer mechanisms. Solutions of polymers in organic solvents are sprayed through a capillary, with CO_2 flowing cocurrently in an annular region about the capillary. The velocities of the two coaxial flows are manipulated independently to better control the process. A high CO_2 velocity in the annulus lowers the relative velocity between the two streams and may be expected to decrease atomization, slowing down mass transfer in the jet. However, the high CO_2 velocity will enhance recirculation and mixing of the suspended droplets throughout the precipitator. Here, we utilize coaxial and standard nozzles to discriminate between the effects of mass transfer in the jet and in the suspension outside of the jet on the final particle size and degree of flocculation. The mass transfer mechanism is investigated in terms of visual imaging of the jet and the product morphology.

The knowledge gained about the mechanism for particle formation is used to examine additional experiments performed with a standard nozzle for three key variables: CO_2 density, polymer concentration, and solvent quality. The effect of liquid CO_2 density on the morphology of L-PLA is compared with previous results at supercritical conditions.[16,21] For L-PLA and PS the polymer concentration is varied from 1.0 to 3.0 wt % to change the mass transfer pathway on the phase diagram. Additional effects of phase behavior are characterized by comparing PS microparticles precipitated

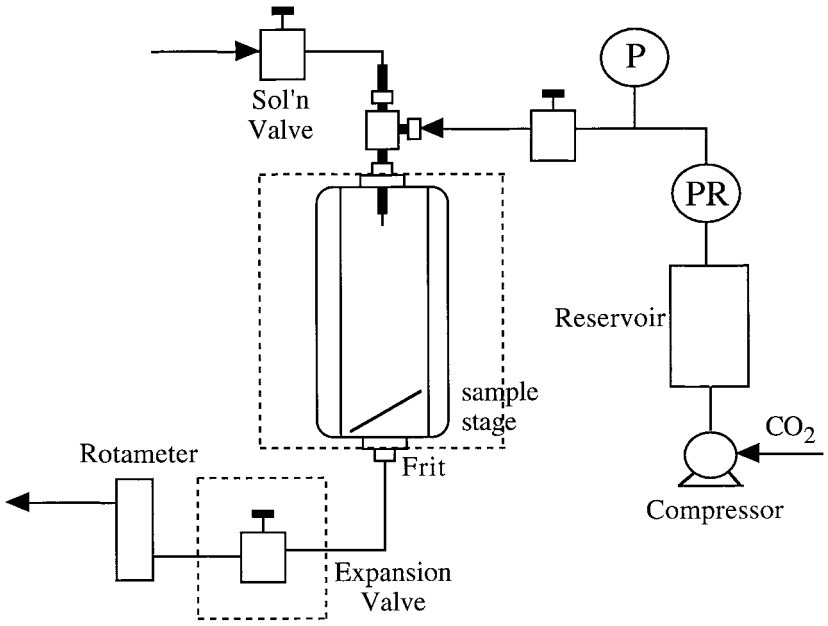

Figure 1 Schematic of the apparatus for precipitation with a compressed fluid antisolvent (PCA).

from tetrahydroduran (THF), to those from a better solvent, toluene.

EXPERIMENTAL

Materials

Monodisperse PS (M_w/M_n = 1.05 i.e., weight average/number average molecular weights) was purchased from Pressure Chemical Inc. and had a molecular weight (MW) of 200,000. Semicrystalline L-PLA (MEDISORB™ 100 L, Stolle–Dupont Co., Cincinnati, OH) had a MW of 94,100 and a M_w/M_n of 1.85. Polyacrylonitrile (PAN) (Aldrich Chemical Company, Inc.) had a MW of 150,000. Reagent grade toluene, THF, methylene chloride, and *N,N*-dimethylformamide (DMF), and instrument grade CO_2 were used as received.

Apparatus

The polymer solution was sprayed into a 1.27 cm i.d., 13-mL sapphire tube to observe the precipitation visually as shown in Figure 1. Details of this vessel and the CO_2 pressurizing assembly have been described elsewhere.[13,20] The CO_2 flowed through a 50-ft long 0.030-in. i.d. × $\frac{1}{16}$-in. o.d. tube in the water bath to raise the temperature to the desired temperature before spraying. Because the CO_2 densities were high, cooling due to the mixing of CO_2 and polymer solution was negligible.

The polymer solution was injected into the CO_2 using a high pressure, computer controlled syringe pump (ISCO pump, model 100D). This pump offered an important advantage over reciprocating pumps, because reciprocating pumps produce undesirable surges in flow with each stroke. The polymer solutions were sprayed through either 50-μm i.d. fused silica capillary tubing (standard nozzle), or a coaxial nozzle consisting of this capillary inserted inside a $\frac{1}{16}$-in. o.d. × 0.030-in. i.d. stainless steel tube as shown in Figure 2. The tip of the capillary tubing protruded approximately $\frac{1}{16}$ in. further into the vessel than the stainless steel sheath. All capillary nozzles were 6.5 in. in length. The capillary tips were inspected with a microscope to insure that they were smooth.

Polymer samples were recovered *in situ* on a small rectangular glass plate ($\frac{1}{4}$ in. × $\frac{1}{8}$ in.), which was sometimes also covered with a piece of double-sided sticky tape. A $\frac{1}{4}$-in. diameter 0.5-μm frit was also placed in the effluent line after the precipitation vessel. Before the experiment, the glass plate was positioned 1–3 in. below the tip of the atomizer and held in place by a plug of stainless steel screen.

A valve in the effluent line (Whitey, SS-21RS4) was used to control the CO_2 flow rate through the

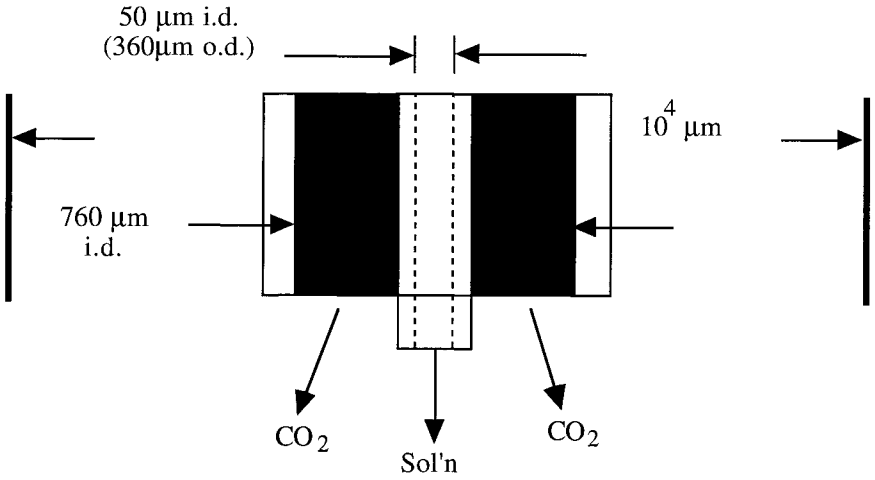

Figure 2 Schematic of the PCA coaxial spray nozzle.

precipitator. The valve was heated in a water bath to prevent freezing due to CO_2 expansion. The CO_2 flow rate was measured with an Omega rotameter (model FLT-40ST). Upon completion of the solution spray, pure CO_2 was pumped through the vessel at a constant flow rate for 10 min to remove any residual organic solvent. After drying, the precipitation vessel was isolated and allowed to depressurize for ~ 15 min. Finally, the glass slide and frit were carefully removed and placed on an SEM stage that was also coated with double-sided sticky tape.

Characterization

Precipitation of a 1.0 wt % PS in toluene solution was recorded with a Panasonic tube video camera (model WV-3240) equipped with a 50-mm Olympus macrolens. A Sony EVO 9700 Hi8 video cassette recorder, which produced sharp still frames, was used to record the precipitation process. Individual still frames were then frozen on a Sony HR Trinitron monitor and photographed.

The morphology of the polymer samples was analyzed and imaged with a Jeol JSM-35C SEM. Samples were sputter coated with gold-palladium to a thickness of approximately 200 Å.

THEORETICAL

To provide a framework for understanding the experimental results, we present a summary of the phase behavior and relevant mass transfer pathways for microparticle formation. Figure 3 shows a schematic phase diagram for a ternary system consisting of polymer, organic solvent, and CO_2. The phase diagram is bounded by three regions: the one-phase region located between the polymer/solvent axis and the binodal line, the metastable region located between the binodal and spinodal lines, and the unstable region located between the spinodal line and the polymer/CO_2 axis. The intersection of the binodal and spinodal curves occurs at the plait point or critical point.

For mass transfer pathways below the plait point, on the polymer lean side of the phase dia-

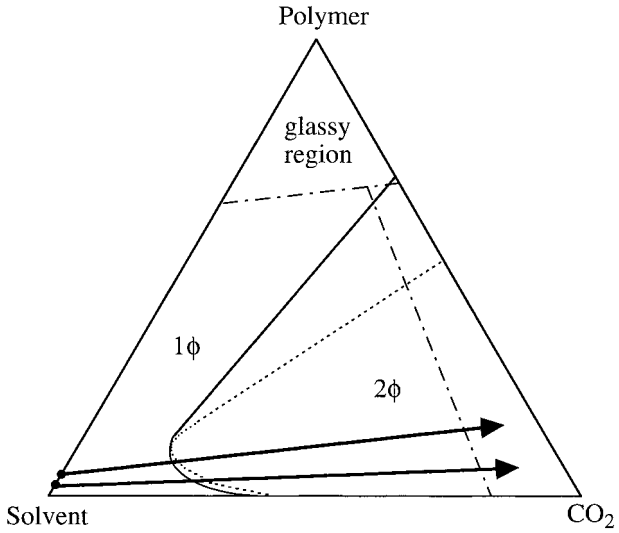

Figure 3 Schematic ternary phase diagram showing the mass transfer pathway for a polymer solution precipitated into compressed CO_2. (—) Binodal line; (---) spinodal line; (- - -) T_g line.

gram, polymer-rich domains nucleate and grow in the metastable region. After the mass transfer pathway crosses the spinodal line, phase separation proceeds by spinodal decomposition. Spinodal decomposition can result in a bicontinuous network of polymer and voids. The polymer-rich domains vitrify at the glass transition temperature, which is depressed by the presence of solvent and CO_2. For CO_2 dissolved in PS at pressures of interest in this study, the temperature must be maintained below 30°C to quench the product in the glassy state.[26] Above 30°C, the primary particles agglomerate into larger domains (i.e., >10 μm) due to plasticization by the CO_2.[14] The presence of toluene further depresses the PS polymer glass transition temperature. For L-PLA, the semicrystalline structure prevents agglomeration from plasticization.[21]

Compared with conventional organic antisolvents, phase separation between the CO_2 phase and solution phase is accelerated with characteristic times down to 10^{-5} cm^2/s.[22] The rates of mass transfer are increased in both directions; for example, the diffusion coefficient of solvent in the continuous phase is 2 orders of magnitude larger in CO_2 than in conventional liquids.

RESULTS AND DISCUSSION

Characterization of PCA Jet Hydrodynamics

Visual observations of the characteristics of the jet provided considerable insight into the mass transfer mechanism. In the first set of experiments, the organic solvent toluene was sprayed into CO_2 at 23°C without any polymer present. For the flow rates investigated (in the ranges discussed later), the solvent mole fraction was always below 0.018 at steady state. For this solvent concentration, each of these solutions was in the one-phase region at equilibrium. For the standard nozzle, small suspended liquid droplets were observed typically after about 5 s. The suspension was identified by a discontinuity in the refractive index at the top of the suspension. The contrast between the suspension and the more dilute region above it was slight but clearly visible to the naked eye. Unfortunately, the contrast was insufficient to see a suspension in the video pictures. For the coaxial nozzle, refractive index gradients were not observed. The solution was completely transparent to the naked eye, indicating suspended droplets were not present. Clearly, the mixing of the atomized droplets and CO_2 throughout the precipitator was much more effective with the coaxial nozzle.

The same type of experiments were repeated with polymer solutions. To characterize these experiments, the dimensionless Reynolds (N_{Re}) and Weber (N_{We}) numbers for a 1.0 wt % PS in toluene solution sprayed into CO_2 are shown in Table II. The N_{We} is the ratio of the inertial forces to surface tension forces and is given by $N_{We} = \rho_A v^2 D/\gamma$ where ρ_A is the antisolvent density, v is the velocity of the jet relative to that of the CO_2, D is the solution jet diameter, and γ is the interfacial tension.[27,28] Jet breakup by atomization is favored when N_{We} is large. In contrast with conventional spray drying, the combination of a high antisolvent density and low interfacial tension between the CO_2 and organic solution creates a large N_{We} for the PCA process. Because γ between the polymer solution and the CO_2 is unknown, and γ changes along the mass transfer pathway, the

Table II Effect of CO_2 Velocity and Nozzle Design on Reynolds and Weber Numbers for 1.0 wt % PS in Toluene Solution Sprayed into CO_2 at 0°C

Nozzle	Q (Solution) (mL/min)	Q (CO_2) (mL/min)	v (Solution) (cm/s)	v (CO_2) (cm/s)	N_{Re} (CO_2)	N_{We} / N_{We} (Q = 90)
Standard	0.5	35	424	0.5	14.	0.25
	1.0	35	849	0.5	14	1.0
	1.5	35	1273	0.5	14	2.25
	1.0	90	849	1.2	35	1.0
Coaxial	1.0	8	849	38	1087	0.91
	1.0	17	849	82	2376	0.82
	1.0	35	849	165	4753	0.65
	1.0	90	849	423	12266	0.25

$\rho_{CO_2} = 0.97$ g/cm^3.

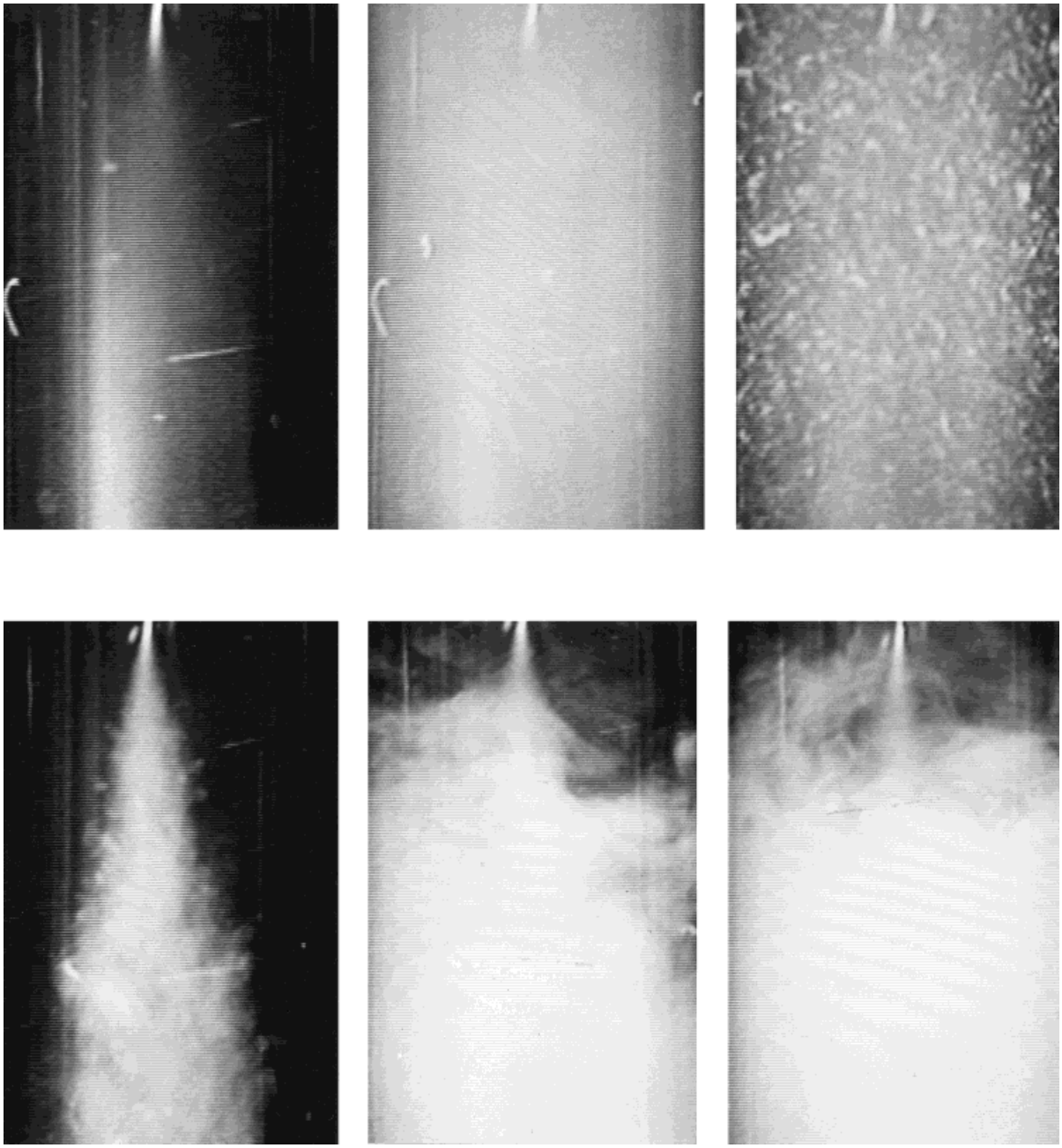

Figure 4 Atomization of a 1.0 wt % PS in toluene solution into CO_2 at 35 mL/min and 23°C (ρ = 0.85 g/cm^3) through 50-μm coaxial (top) and standard (bottom) spray nozzles at 1, 5, and 10 s.

N_{We} values are normalized by the value for a 90 mL/min CO_2 flow rate with the standard nozzle, assuming γ is constant.

The results of spraying a 1.0 wt % PS in toluene solution at 1.0 mL/min into CO_2 at 23°C are shown for spray times of $<$1, 5, and 10 s for the coaxial (Fig. 4, top) and standard (Fig. 4, bottom) nozzles. The CO_2 flow rate was maintained at 35 mL/min. In the first second of the spray, the cloud of PS-rich precipitate was much smaller for the coaxial nozzle than the standard one. The faster precipitation in the jet for the standard nozzle is due to smaller droplets resulting from more intense atomization. The stronger atomization is due to the larger relative N_{We} resulting from the larger relative velocity.

After 5 s of spraying with the standard nozzle, a dense cloud of precipitate builds up from the bottom of the vessel to the tip of the capillary. Above this suspension, the solution is relatively clear. The suspension did not fill the entire vessel, and the particles did not appear to recirculate very rapidly, indicating poor mixing. Refractive index gradients appeared, indicating the initial formation of a suspension of clear liquid droplets. In contrast, the precipitate from the coaxial nozzle recirculated rapidly throughout the entire vessel, due to the much larger N_{Re}. For the coaxial nozzle clear liquid droplets were not present, only white precipitate.

After 10 s of spraying with the standard nozzle, the particles still did not mix with the clear solution above the precipitate. The refractive index gradients at 5 s evolved into an apparent meniscus of solvent droplets that was easily observed with the naked eye in addition to a large mass of suspended white precipitate. The elapsed time for the initial formation of these droplets, typically <5 s, depended upon the solution flow rate, but not the solute concentration. The poor mixing outside of the jet due to a small N_{Re} and laminar CO_2 flow slows two-way mass transfer of solvent out of and CO_2 into the suspended droplets. Consequently, solvent-rich droplets were prevalent throughout the precipitator.

In contrast, clear liquid droplets were not present for the coaxial nozzle even at 10 s, and the precipitate appeared to be dry. Here the N_{Re} was much larger and the flow became turbulent. The convective mass transport in the suspension was much more rapid than for the standard nozzle. In summary, for the coaxial nozzle versus the standard one, the mass transfer in the jet appears to be slower in delaying precipitation and the mass transfer in the suspension appears to be faster, leading to more complete mixing and drying of the suspended particles that left the jet.

For the coaxial nozzle, significant flocculation and agglomeration took place as indicated by the large particles observed throughout the precipitator in the top of Figure 4 (10 s). Similar large particles could also be seen for the standard nozzle, but they were much less prevalent. These ob-

Table III Polymer Morphology Produced by Spraying Homogenous Solutions of Amorphous Polystyrene in Toluene, Semicrystalline L-PLA in CH_2Cl_2, and Semicrystalline Polyacrylonitrile in DMF into Carbon Dioxide at 35 mL/min

Polymer	$C_{sol'n}$ (wt %)	T (°C)	ρ (CO_2) (g/cm^3)	Nozzle Design	Q (Solution) (mL/min)	Primary Particles (μm)	Microparticle Macrostructure
PS	1.0	23	0.85	Std.	0.5, 1.0, 1.5	0.5–1.0	Flocc./sl. agglom.
	1.0	0	0.96	Std.	1.0	0.5–1.0	Flocc./sl. agglom.
	1.0[a]	0	0.96	Std.	1.0	0.1–0.3	Flocc./sl. agglom.
	3.0	0	0.96	Std.	1.0	0.1–0.3	Flocc./sl. agglom.
	1.0	0	0.96	Coaxial	1.0	0.5–5.0	Ind./sl. flocc.
	1.0	23	0.85	Coaxial	0.5, 1.0[b]	0.5–10.0[c]	Ind./sl. flocc.
	1.0	23	0.85	Coaxial	1.0	0.1–1.0[d]	Ind./sl. flocc.
	3.0	23	0	Coaxial	1.0	0.1–0.5	Flocc./sl. agglom.
L-PLA	1.0	23	0.85	Std.	0,5 1.0	0.5–2.0	Sl. flocc./sl. agglom.[e]
	1.0	26	0.75	Std.	1.0	0.5–4.0	Sl. flocc./sl. agglom.[e]
	1.0	0	0.96	Std.	1.0	0.1–1.0	Sl. flocc./sl. agglom.[e]
	3.0	23	0.85	Std.	1.0	0.1–1.0	Sl. flocc./sl. agglom.[e]
	1.0	23	0.85	Coaxial	0.5, 1.0	0.5–5.0[c]	Ind./sl. flocc.
	3.0	23	0.85	Coaxial	1.0	0.1–1.0	Ind./sl. flocc.
PAN	0.5	40	0.66	Std.	1.0	0.1–0.3	No. flocc./agglom.[f]
	0.5	40	0.66	Coaxial	1.0	0.1–0.3	No. flocc./agglom.[c,g]

[a] THF used as a solvent.
[b] 2.0–5.0 μm microparticles also produced when Q (CO_2) = 17 mL/min.
[c] Bimodal particle size distribution.
[d] Q (CO_2) = 8 mL/min.
[e] Agglomerates when spray $>$ 10 s.
[f] Oriented fibrils.
[g] Oriented fibrils, individual fibrils, and microparticles.

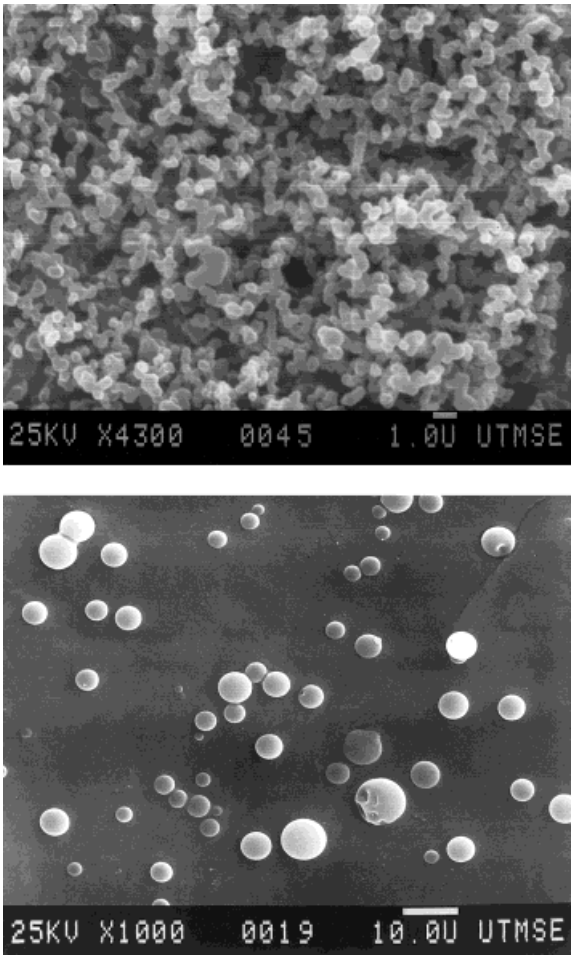

Figure 5 SEM micrographs of PS formed by spraying a 1.0 wt % PS in toluene solution at 1.0 mL/min through 50-μm standard (top) and coaxial (bottom) spray nozzles into CO_2 at 35 mL/min and 0°C (ρ = 0.96 g/cm^3).

servations will be interpreted after discussing the product morphologies from SEM.

Effect of Nozzle Design on Microparticle Morphology

A summary of the various morphologies produced by the coaxial and standard atomization nozzles is shown in Table III. When a 1.0 wt % PS in toluene solution is sprayed through the standard nozzle, intense atomization produces small droplets based on visual observation. Mass transfer is expected to be very fast for the small droplets, as further indicated by the formation of small 0.5–1.0 μm primary particles shown in Figure 5 (top). Figure 3 (bottom, <1 s) shows that the particle density is large in the jet, and it is likely that these particles begin to flocculate not far from the capillary tip. In contrast, the mass transfer in the suspension outside the jet is slow due to laminar flow of CO_2 (low N_{Re}). The small primary particles leaving the jet are dried very slowly because of poor recirculation. Because of the slow drying, the particle collisions lead to further flocculation and partial agglomeration, as shown in Figure 4. As stated above, solvent-rich liquid droplets are visible at <5 s into the spray, indicating poor mixing in the suspension.

For the same conditions, except with the coaxial nozzle, weaker atomization leads to larger droplets in the jet. The two-way mass transfer takes longer for the larger droplets, and precipitation within the jet is delayed compared with the standard nozzle. Because the large droplets are relatively wet in the jet, coalescence is more prevalent than for the smaller dryer particles produced by the standard nozzle. Consequently, much larger and more spherical particles are formed by the coaxial nozzle as shown by Figure 5 (bottom). After leaving the jet, mass transfer is faster in the suspension for these particles due to the larger N_{Re}. They are more uniformly recirculated throughout the view cell and dry more rapidly without flocculating. The particle density is much smaller in the suspension than in the jet, because of the larger volume and the decrease in the number of particles after coalescence in the jet. Thus, flocculation may be expected to be less likely in the suspension than in the jet.

For longer times for the coaxial sprays, at a given polymer concentration and solution flow rate, the PS microparticles flocculate once a critical concentration of particles accumulates within the precipitator. After about 10 s these flocculates agglomerate to produce >50-μm particles based on SEM micrographs (not shown). It is likely that this critical flocculation time depends upon the stickiness of the plasticized polymer. For example, semicrystalline L-PLA is much less sticky than amorphous PS in the presence of CO_2, because the crystalline domains reduce plasticization. Unlike PS,[14] L-PLA does not flocculate or agglomerate when exposed to CO_2 at temperatures as high as 40°C.[21,29]

Figure 6 shows the microparticles formed by spraying a 1.0 wt % L-PLA in methylene chloride solution at 1.0 mL/min into CO_2 at 35 mL/min. For the standard nozzle (Fig. 6, top) 0.5–1.0 μm particles are produced with little flocculation. As expected, the particles are less plasticized by CO_2 than the PS particles and have a much smaller tendency to flocculate. With the coaxial nozzle

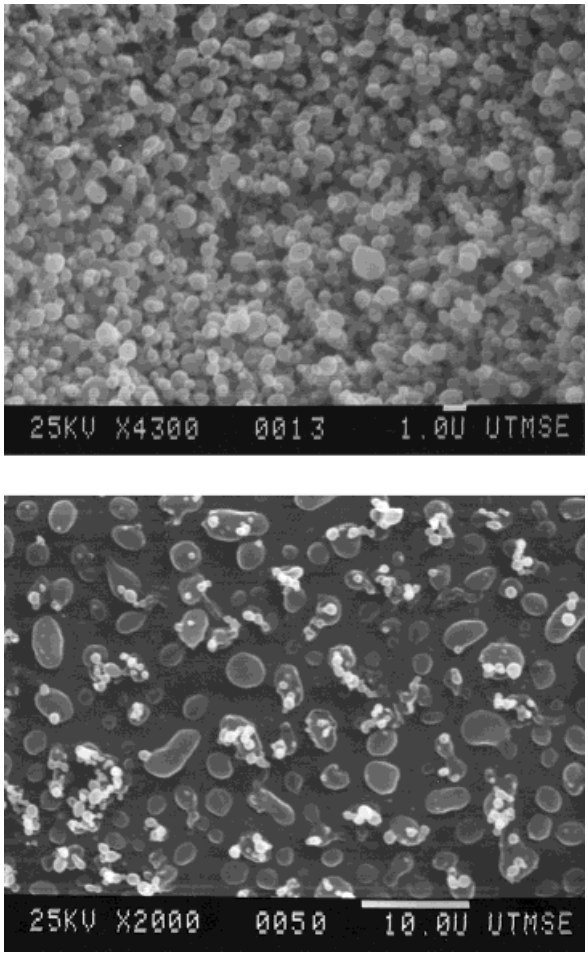

Figure 6 SEM micrographs of semicrystalline L-PLA microspheres formed by spraying a 1.0 wt % L-PLA in methylene chloride solution at 1.0 mL/min through 50-μm standard (top) and coaxial (bottom) spray nozzles into CO_2 at 35 mL/min and 23°C (ρ = 0.85 g/cm^3).

much larger 2–5 μm L-PLA microparticles are precipitated along with 0.5–1 μm particles. Again the slower jet mass transfer delays precipitation leading to larger particles. The bimodal size distribution may suggest the formation of particles in the jet and in the suspension. For the standard nozzle, slow drying of the particles in the suspension lead to flocculation and agglomeration.

The difference in flocculation for the coaxial and standard nozzles is accentuated for longer spray times where solvent can accumulate. A 1.0 wt % L-PLA in methylene chloride solution at 1.0 mL/min was atomized into CO_2 at 35 mL/min for >12 s. Figure 7 (top) shows 0.5–1.0 μm L-PLA microparticles with the flocculation obtained with the coaxial atomizer. In contrast, highly agglomerated microparticles are precipitated by the standard atomization nozzle (Fig. 7, bottom). Unlike the case for the coaxial nozzle, a discernible meniscus of "foglike" solvent-rich droplets was observed. Once the solution spray was stopped, the fog descended and fully disappeared. The large buildup of wet droplets in the suspension led to severe agglomeration.

To further explore the mass transfer mechanism in PCA, we studied PAN in DMF solutions. PAN has a strong tendency to form fibers due to strong dipole–dipole interactions. PAN was previously shown to form oriented microfibrils with a standard nozzle.[20] Our goal was to prevent fiber formation and to form particles by manipulating the hydrodynamics and mass transfer.

Figure 8 shows the results of spraying a 1.0 wt % PAN in DMF solution at 1.0 mL/min into CO_2 flowing at 35 mL/min. With the standard nozzle

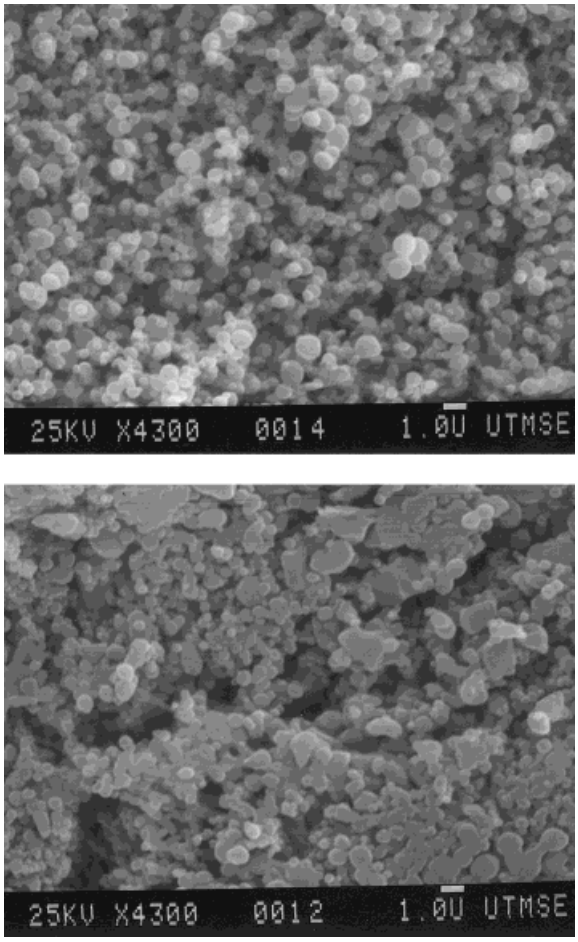

Figure 7 SEM micrographs of L-PLA microspheres formed by spraying a 1.0 wt % L-PLA in methylene chloride solution at 1.0 mL/min through 50-μm coaxial (top) and standard (bottom) spray nozzles into CO_2 at a flow rate of 35 mL/min and 23°C (ρ = 0.85 g/cm^3).

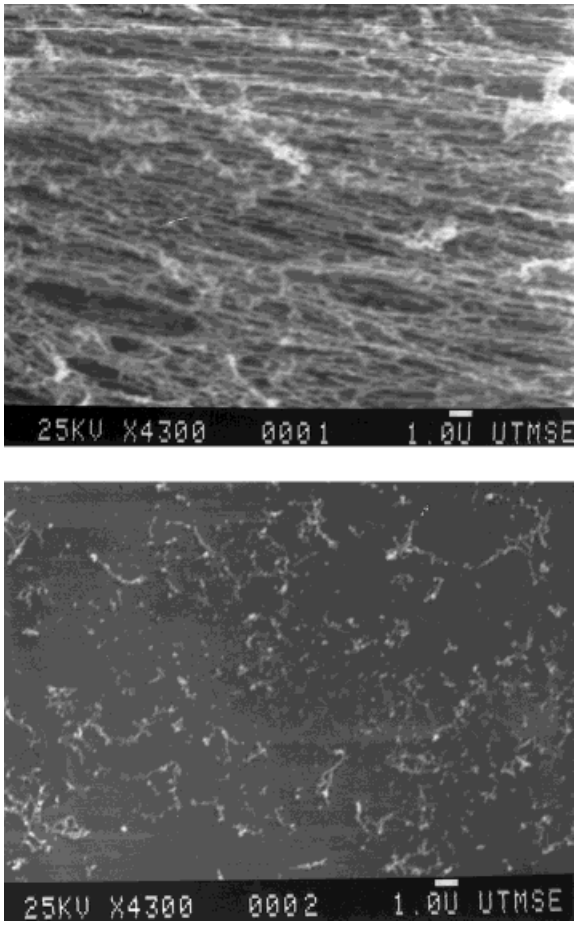

Figure 8 SEM micrographs of oriented (top) and individual (bottom) semicrystalline PAN fibrils formed by spraying a 1.0 wt % PAN in DMF solution at 1.0 mL/min through a 50-μm coaxial spray nozzle into CO_2 at 35 mL/min and 40°C (ρ = 0.66 g/cm^3).

(Fig. 8, top), continuous, highly oriented microfibrils are formed as observed previously. These microfibrils are oriented by shear forces that arise from the high velocity of the solution relative to CO_2.[20] Because the primary particles in the microfibrils are only 0.1–0.3 μm in diameter and are highly interconnected, it is likely the microfibrils begin to form early in the jet where the particle density is high. Microfibrils are also present in experiments with the coaxial nozzle (not shown). However, much shorter and less oriented individual PAN fibrils and microparticles are also observed (Fig. 8, bottom), which were not formed by the standard nozzle. Because of the delayed precipitation due to the lower N_{We} in the jet, the jet breaks up before the high shear and high local polymer density would otherwise cause all of the product to be in the form of oriented fibrils. The smaller size of these particles relative to those of the other polymers may be due to less sticky particle collisions, because of the high degree of crystallinity that limits CO_2 sorption.[20]

Effect of Density on Microsphere Morphology

Because the effect of density on particle size is not well understood, we reexamine this issue given the above newly gained knowledge about the PCA mass transfer mechanism. Figure 9 shows L-PLA microparticles precipitated at a CO_2 density of 0.96 g/cm^3 (T = 0°C) (top) and 0.75 g/cm^3 (T = 26°C) (bottom), respectively. (Below the critical temperature of CO_2 it was necessary to vary the temperature to change the density by this large amount.) For both experiments, the

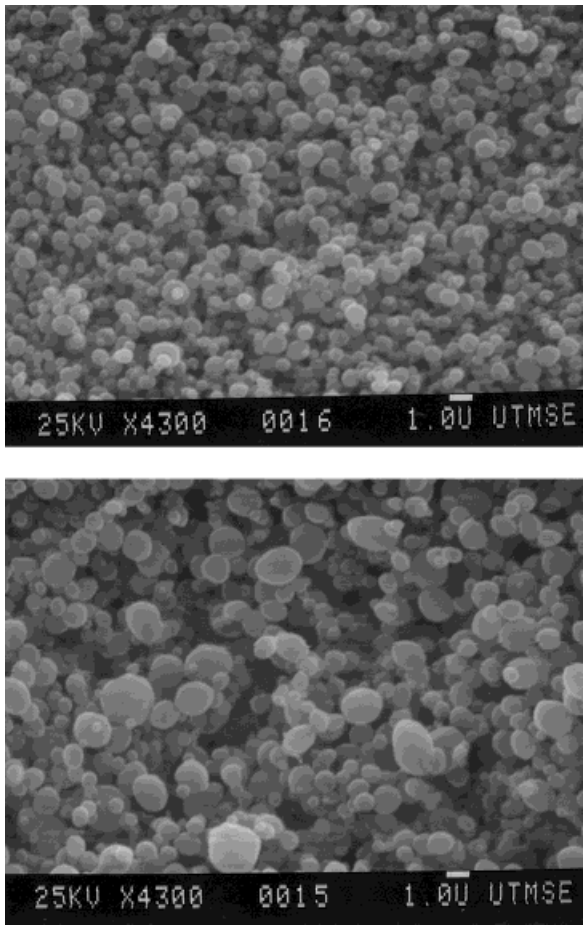

Figure 9 SEM micrographs of semicrystalline L-PLA microspheres formed by spraying a 1.0 wt % L-PLA in methylene chloride solution at 1.0 mL/min through a 50-μm standard spray nozzle into CO_2 at a flow rate of 35 mL/min and a density of 0.96 g/cm^3 (T = 0°C) (top) and 0.75 (T = 26°C) (bottom).

standard nozzle was utilized with solution and CO_2 flow rates of 1.0 and 35 mL/min, respectively. The SEM images are from a L-PLA sample collected on the 0.5-μm frit as shown in Figure 1. An increase in particle size from 0.1–1.0 to 0.1–3.0 μm is observed with decreasing CO_2 density, in agreement with previous results.[21] For a lower CO_2 density and lower N_{We}, larger droplets are produced during jet atomization. For a constant mass transfer rate, larger droplets allow more time for growth of the polymer-rich domains. Consequently, larger microparticles are produced.

In contrast, Randolph et al.[16] observed an increase in particle size from 0.61 to 1.4 μm with an increase in CO_2 density from 0.65 to 0.76 g/cm^3 when a 0.6 wt % L-PLA solution was sprayed though a sonicator into CO_2 at 31°C. Similar results were obtained at 36 and 40°C. Randolph et al.[16] suggested that smaller particles are produced as the diffusion coefficients of the solvent in CO_2 increase, that is, at lower densities. Faster mass transfer rates (higher diffusion coefficients) lead to increased supersaturation and faster nucleation rates. Consequently, smaller particles are produced.

The apparently conflicting results of these two studies may be resolved by comparing the effects of atomization and mass transfer. The behavior of the diffusion coefficient of the solvent in CO_2 will basically follow that of pure CO_2. When the conditions of CO_2 are changed from 0°C and 80 bar (0.96 g/cm^3) to 26°C and 110 bar (0.75 g/cm^3), D changes from 7.0×10^{-5} to 1.0×10^{-4} cm^2/s. At 31°C, D increases from 2.5×10^{-4} to 1.0×10^{-3} cm^2/s as the pressure is decreased from 95 to 62 bar.[30] In the study of Randolph et al.[16] the increase in mass transfer from the larger increase in D as density decreases, accelerates the phase separation leading to smaller particles. In our study, the effect of atomization is dominant, because the change in D is smaller at subcritical conditions. Consequently, particle size decreases with density.

Effect of Phase Behavior on Microsphere Morphology

Polymer Concentration

All of the experiments in this section were performed with the standard nozzle. PS and L-PLA solutions, each at 3.0 wt %, were sprayed at 1.0 mL/min into CO_2 at 35 mL/min as shown in Figure 10. The average size of the resulting PS microparticles (top) formed at 0°C and ρ = 0.96 g/cm^3 was 0.1–0.3 μm. These microparticles are significantly smaller than the 0.5–1.0 μm microparticles produced at similar conditions for a 1.0 wt % solution (see Fig. 5, top). The same behavior was observed for L-PLA. For the L-PLA microparticles produced from a 3.0 wt % solution shown in Figure 10 (bottom), most of the particles were in a size range of 0.1–0.5 μm, with a few larger 1.0-μm microparticles. For comparison, the typical particle size for a 1.0 wt % solution at 0°C (ρ = 0.96 g/cm^3) was 0.5–1.0 μm, a much larger value (see Fig. 9 top).

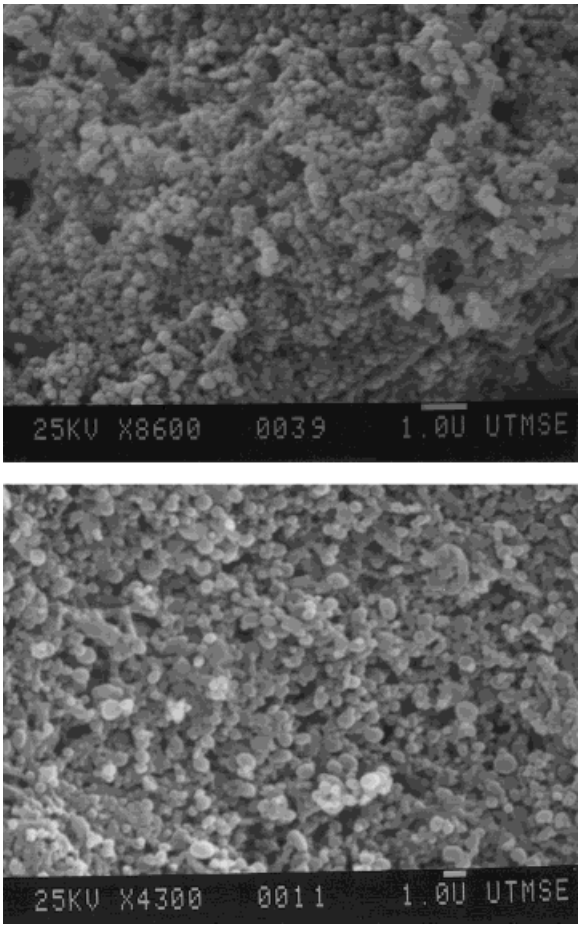

Figure 10 SEM micrographs of PS microspheres formed by spraying a 3.0 wt % PS (0°C, 0.96 g/cm^3) in toluene (top) and L-PLA (23°C, 0.85 g/cm^3) in methylene chloride solution (bottom) at 1.0 mL/min through a 50-μm standard spray nozzle into CO_2 at 35 mL/min.

The observed decrease in particle size with an increase in solute concentration may at first seem counterintuitive, but may be explained by analyzing the ternary phase diagram shown in Figure

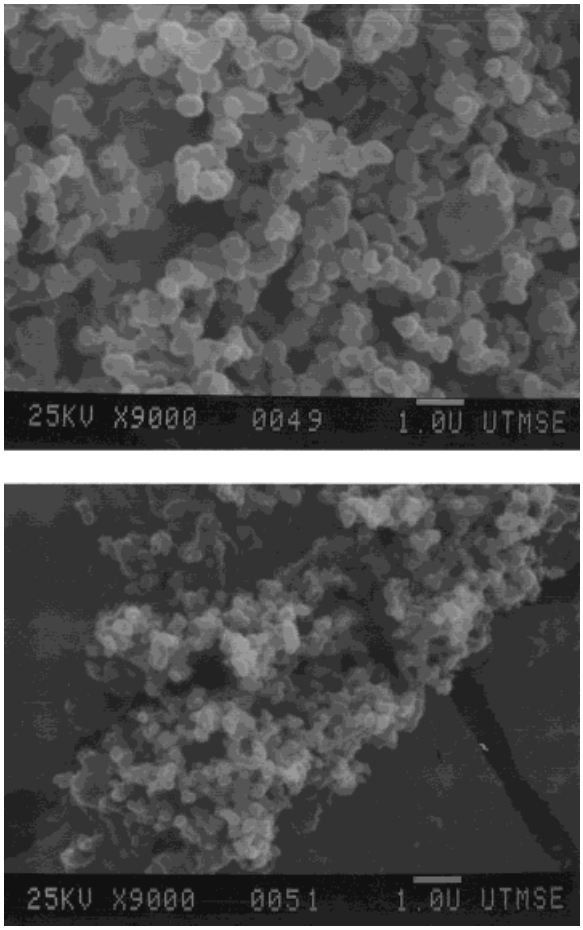

Figure 11 SEM micrographs of PS microspheres formed by spraying a 1.0 wt % PS in toluene (top) and THF (bottom) solution at 1.0 mL/min through a 50-μm coaxial spray nozzle into CO_2 at 35 mL/min and 0°C (0.96 g/cm^3).

3. As the polymer concentration increases from 1 wt % (represented by pathway A) to 3 wt % (B), the mass transfer pathway shifts toward the plait point. Consequently, the distance between the binodal and spinodal curves decreases. Thus, the time for growth of polymer-rich domains in the metastable region decreases, resulting in smaller particles as observed by comparing Figures 5 (top) and 10 (top). This explanation is supported by visual observations of the initial part of the sprays, because the 3.0 wt % PS solution precipitated sooner than the 1.0 wt % solution.

Solvent Quality

The solvent quality is another variable for controlling the particle size. To produce smaller microparticles from a 1.0 wt % PS solution, toluene was replaced with a poorer solvent, THF. Figure 11 (bottom) shows 0.1–0.3 μm PS microparticles formed by spraying a 1.0 wt % PS in THF solution at 1.0 mL/min into CO_2 at 35.0 mL/min through the standard nozzle. The particle size is significantly smaller than the 0.5–1.0 μm microparticles produced from toluene solution shown in Figure 11 (top). The particles resemble those from 3.0 wt % PS in toluene solutions shown in Figure 10 (top).

The solubility parameters for toluene and THF are 8.9 and 9.1 (cal/cm^3)$^{1/2}$, respectively. From visual observations made with a variable-volume view cell apparatus described elsewhere,[11] the solubility limit of CO_2 in various polymer solutions was measured. The point at which the polymer precipitated was determined. At 0°C and 110 bar (0.95 g/cm^3), a 1.0 wt % PS/THF solution precipitated with the addition of 41.7 wt % CO_2 whereas 46.9 wt % CO_2 was required to precipitate a 1.0 wt % PS/toluene solution. Because THF is a poorer solvent for PS, less CO_2 is needed for precipitation. The larger two-phase envelope for THF is illustrated schematically in Figure 12. Because the polymer precipitates sooner in the jet for THF, smaller particles are produced. This trend was established above in comparing the standard and coaxial nozzles. It is unknown how the distance between the binodal and spinodal varies between these two systems; it would be interesting to determine this in the future.

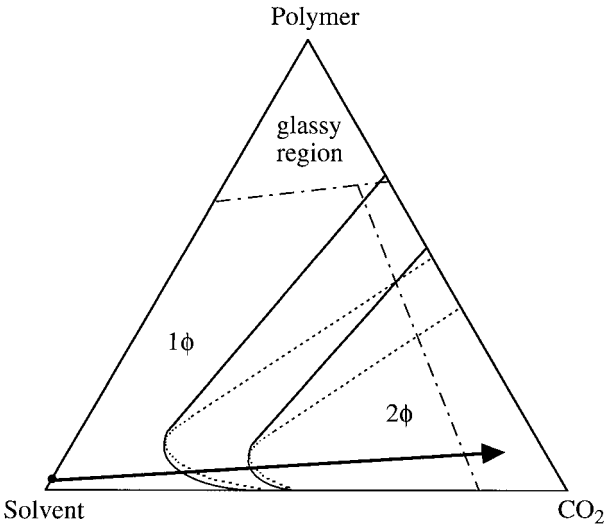

Figure 12 Ternary phase diagram showing the effect of solvent quality upon the two phase envelope and the mass transfer pathway for a PS solution precipitated into compressed CO_2. (—) Binodal line; (---) spinodal line; (– – –) T_g.

CONCLUSIONS

For the coaxial versus the standard nozzle, polymer particles can be larger by a factor of 3–8 with far less flocculation. Because N_{We} is smaller, atomization is less intense and larger droplets are formed in the jet delaying precipitation. However, because of the much higher N_{Re} for the high velocity CO_2, the mass transfer in the suspension is faster leading to less flocculation and agglomeration.

Our proposed mechanism is supported by direct visual observation in addition to the product morphology. For the standard nozzle, initial precipitation is faster due to more intense atomization. However, the resulting suspension does not fill the entire vessel and the particles do not recirculate very rapidly, indicating poor mixing. In contrast, for the coaxial nozzle initial precipitation is delayed, but the suspended particles recirculate rapidly throughout the entire vessel.

For PS and L-PLA the coaxial nozzle led to larger particles, from 2 to 10 μm, with much less flocculation than produced by the standard nozzle. For PAN the coaxial nozzle produces a transition from highly oriented continuous microfibrils to individual microparticles on the order of 0.1–0.3 μm. Because of the delayed precipitation, the jet breaks up before the high shear and the high local polymer density can produce oriented fibers.

For the standard nozzle the effects of solvent density, polymer concentration (below the plait point), and solvent quality have been explained on the mass transfer pathways. The solvent density influences the particle size of L-PLA due to two competing effects: changes in atomization and in diffusion coefficients. At subcritical temperatures where changes in diffusion coefficients are relatively small, the effect of atomization is dominant. Here the atomization (N_{We}) becomes more intense as density increases and the particle size decreases. At supercritical temperatures the opposite behavior has been observed[16] because the diffusion coefficient effect is dominant.

The size of PS and L-PLA microparticles decreases by a factor of 3–10 with an increase in polymer concentration from 1.0 to 3.0 wt %, as the width of the metastable region decreases. Less time is available for growth for polymer-rich domains. By replacing toluene with a solvent of poorer quality, THF, the size of PS is reduced by a factor of 3–8 also. Because the size of the two-phase region is larger for THF, the polymer precipitates sooner in the jet, leading to the smaller particles.

The authors are grateful for support from NSF (CTS-9218769), the Texas Advanced Technology Program (3658-198), and the Separations Research Program at The University of Texas. The authors thank Ron Rousseau for stimulating ideas concerning mass transfer in the suspension, and also thank ISCO Corporation for the donation of the high pressure syringe pump. Finally, the authors also thank Ralf Lukner for the use of the video equipment.

REFERENCES

1. R. Dagani, *Chem. & Eng. News,* 33 (December 19, 1994).
2. R. L. Juliano, Ed., *Controlled Drug Delivery: Fundamentals and Applications,* Marcel Dekker, New York, 1987, p. 550.
3. L. Hixon, M. Prior, H. Prem, and J. Van Cleef, *Chem. Eng.,* 94 (November, 1990).
4. D. W. Matson, J. L. Fulton, R. C. Peterson, and R. D. Smith, *Ind. Eng. Chem. Res.,* **26,** 2298 (1987).
5. J. W. Tom and P. G. Debenedetti, *J. Aerosol Sci.,* **22,** 555 (1991).
6. E. M. Phillips and V. J. Stella, *Int. J. Pharmaceut.,* 1 (1992).
7. S. N. Boen, M. D. Bruch, A. K. Lele, and A. D. Shine, in *Polymer Solutions, Blends, and Interfaces,* I. Noda and D. N. Rubingh, Eds., Elsevier Science Publishers B.V., Amsterdam, 1992, p. 151.
8. A. K. Lele and A. D. Shine, *AICHE J.,* **38,** 742 (1992).
9. A. K. Lele and A. D. Shine, *Ind. Eng. Chem. Res.,* **33,** 1476 (1994).
10. J. W. Tom, P. G. Debenedetti, and R. Jerome, *J. Supercrit. Fluids,* **7,** 9 (1994).
11. S. M. Mawson, K. P. Johnston, J. R. Combes, and J. M. DeSimone, *Macromolecules,* **28,** 3182 (1995).
12. P. M. Gallagher, M. P. Coffey, V. J. Krukonis, and N. Klasuts, in *Supercritical Fluid Science and Technology,* Vol. 406, K. P. Johnston and J. M. L. Penninger, Eds., American Chemical Society, Washington, D.C., 1989, p. 334.
13. D. J. Dixon, Ph.D. dissertation, The University of Texas at Austin, 1992.
14. D. J. Dixon, R. A. Bodmeier, and K. P. Johnston, *AIChE J.,* **39,** 127 (1993).
15. D. J. Dixon and K. P. Johnston, *J. Appl. Polym. Sci.,* **50,** 1929 (1993).
16. T. W. Randolph, A. D. Randolph, M. Mebes, and S. Yeung, *Biotechnol. Prog.,* **9,** 429 (1993).
17. S.-D. Yeo, P. G. Debenedetti, M. Radosz, and H.-W. Schmidt, *Macromolecules,* **26,** 6207 (1993).
18. S. Yeo, G. Lim, P. G. Debenedetti, and H. Bernstein, *Biotechnol. Bioeng.,* **41,** 341 (1993).

19. D. J. Dixon, G. Luna–Bàrcenas, and K. P. Johnston, *Polymer,* **35,** 3997 (1994).
20. G. Luna–Bàrcenas, S. K. Kanakia, I. C. Sanchez, and K. P. Johnston, *Polymer,* **36,** 3173 (1995).
21. R. Bodmeier, H. Wang, D. J. Dixon, S. Mawson, and K. P. Johnston, *Pharmaceut. Res.,* **12,** 1211 (1995).
22. S. Mawson, S. Kanakia, and K. P. Johnston, *Polymer,* to appear.
23. J. M. DeSimone, Z. Guan, and C. S. Elsbernd, *Science,* **257,** 945 (1992).
24. A. K. Lele and A. D. Shine, *Polym. Prepr.,* **31,** 677 (1991).
25. R. Falk, T. Randolph, J. D. Meyer, R. M. Kelly, and M. C. Manning, *Pharmaceut. Res.,* submitted.
26. P. D. Condo, D. R. Paul, and K. P. Johnston, *Macromolecules,* **27,** 365 (1994).
27. A. H. Lefebvre, *Atomization and Sprays,* Hemisphere Publishing Corporation, New York, 1989.
28. L. Bayvel and Z. Orzechowski, *Liquid Atomization,* Taylor and Francis, Washington, D.C., 1993.
29. H. Wang, M.S. dissertation, The University of Texas at Austin, 1993.
30. M. A. McHugh and V. J. Krukonis, *Supercritical Fluid Extraction Principles and Practice,* 2nd ed., Butterworths, Stoneham, MA, 1994.